# FDTD Analysis of the Radiometric Temperature Measurement of a Bilayered Biological Tissue Using a Body-Contacting Waveguide Probe

Lin-Kun Wu, *Member, IEEE*, and William K. Nieh

***Abstract*—Radiometric signal received by an open-ended rectangular waveguide probe in direct contact with a bilayered biological tissue is analyzed by the FDTD method. Two-layer tissue model consists of an outer thin skin layer over a semi-infinite fat layer is analyzed for a *X*-band total power radiometer. A spherical tumor with same permittivity as, but slightly higher temperature than, the surrounding normal fat tissue is assumed to exist inside the fat tissue. Active probe characteristics are analyzed first using the FDTD method for a propagating, sinusoidally time-varying, $TE_{10}$ type of excitation source. For the same waveguide probe operated as the radiometer antenna, radiometric weighting factors associated with individual tissue cells are then derived from the FDTD calculated field values. Near field radiating characteristics of the probe and radiometric signals determined for tumors of various size and depth are discussed. Presence of the skin is found to result in lower power transmission coefficient across the probe aperture and significantly lower absorbed powers by fat; both of these contribute to much lower radiometric signals observed.**

## I. Introduction

DEVELOPMENT of microwave radiometry for use as a noninvasive breast cancer detection technique has received a great deal of attentions over the past 20 years [1]–[13]. Radiometric detection is feasible because a malignant tumor is known to be hotter than the surrounding tissue under normal condition [14] and, as shown in [15], even higher temperature differential can be achieved by application of electromagnetic energy to heat tumor region.

Taking into account the intensity of thermal emission and tissue loss, microwave radiometers usually operate in the 1–10-GHz frequency range and dielectric-filled waveguide probes placed in direct contact with the body surface are usually employed to achieve better impedance matching and coupling into the body [16], [17]. Thermal energy emitted from lossy body tissue residing in the near-field region of the radiometer antenna is received. To determine radiometric signal, the near fields radiated by radiometer antenna operating in transmission mode are calculated first. Because of antenna reciprocity, the fraction of energy absorbed by each individual tissue cell determined in this active process equals the percentage of energy emitted from the same tissue volume that is received by the same probe operating as radiometer antenna [5]–[7], [11], [12], [18]. Therefore, analysis of the near fields radiated by a body-contacting radiometer antenna is central to the design and performance evaluation of microwave radiometer for detecting a subcutaneous malignant breast tumor.

Guy [19] employed a Fourier transform (i.e., spectral) approach to predict near fields induced in a bilayered biological tissue media in direct contact with a given aperture source field distribution. A two-layer tissue model consisting of an outer fat layer over a semi-infinite inner muscle layer was considered while the effects of skin were ignored. Since only large-sized aperture sources were considered, its results are applicable only to scenarios involving diathermic heating of the areas of the body having relatively large flat surface (e.g., flat shoulder, chest, and back areas). In [20], Alanen and Lindell applied the exact image theory to analyze effects of skin in radiometric detection of cancerous breast tumor at 5 GHz (note that [20] actually considered only the active process involved). Tumor is assumed to have same permittivity as the surrounding fatty breast tissue. Ideal single- and multiwaveguide-mode type of aperture source functions, were considered. Effects of reflecting $TE_{10}$ and higher-order TE- and TM-mode were ignored in [19] and [20].

In [21], the integral equation method was used to solve reflection and transmission problems associated with a flanged, open-ended, monomode rectangular waveguide in direct contact with parallely layered lossy dielectric media. Reflection and cross polarization effects were accounted for by the use of appropriate dyadic Green's functions inside and outside the waveguide. However, this approach is rather complicated and dependent upon the specific layer structure considered. A similar lossy-half space problem was analyzed by Mamouni *et.al.* [5], [6] using a hybrid modal-spectral method; the method was extended recently to the multilayered problem [7].

In this paper, the FDTD method [22] is used to compute the radiometric signal received by a flanged, open-ended, rectangular waveguide in direct contact with a bilayered breast tissue model. In particular, operation of a conventional *X*-band total-power radiometer is simulated. Issues concerning the use of a method previously reported in [23] for compensating the effects of reflection off the probe aperture on radiometric sensing of a semi-infinite lossy medium to the present two-layer problem will also be discussed briefly. For the dual purpose of improving impedance matching and reducing antenna footprint (which is essential to realizations

Manuscript received August 4, 1994; revised January 12, 1995. This work was supported by the National Science Council of the Republic of China Grant NSC82-0115-E009-418.

The authors are with the Institute of Communication Engineering, National Chiao Tung University, Hsinchu, Taiwan 30050, Republic of China.

IEEE Log Number 9412047.

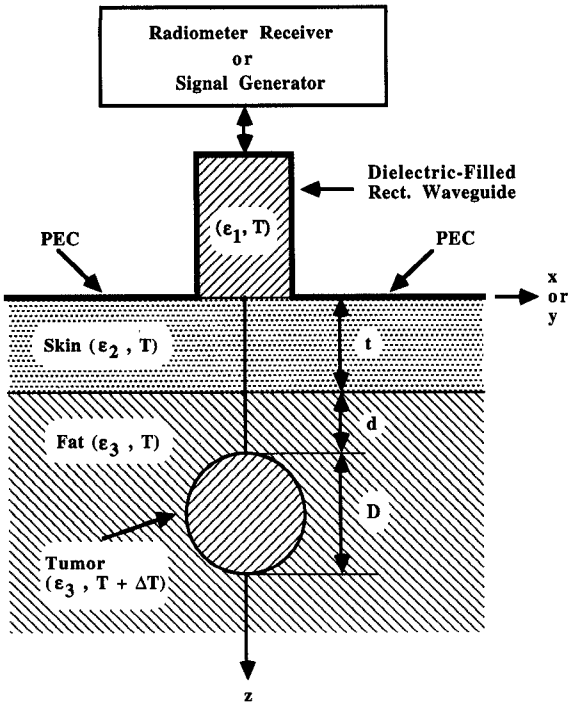


Fig. 1. Problem geometry for both active and passive processes.

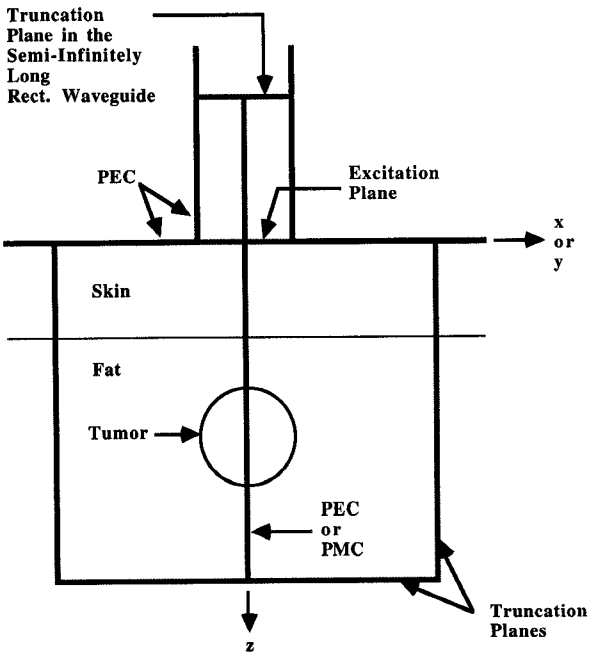


Fig. 2. Specification of FDTD problem space.

of two-probe correlation radiometer [5], [6], [9], [24] and multiprobe aperture-synthesis radiometer [10]–[12]), use of an alumina-filled rectangular waveguide is considered. Two plane layers tissue model consists of a thin skin layer above a semi-infinite fat layer is analyzed. For simplicity, a spherical tumor having the same permittivity as, but is slightly higher in temperature than, the surrounding normal fat tissue is considered. Fig. 1 illustrates the geometry of the problem to be considered.

## II. Method of Analysis

In this study, computation of radiometric signal proceeds in two steps [5]–[7], [18]: 1) determine the reflection and radiation characteristics of the waveguide probe using FDTD, and 2) determine the radiometric weighting factors for all tissue cells when the same probe is used as radiometer antenna.

### A. FDTD-Based Field Analysis

To facilitate FDTD-based field analysis of the radiating probe, a finite-sized FDTD problem space has to be selected out of the original problem geometry. The FDTD lattice shown in Fig. 2 consists of a finite-lengthed lossless waveguide region and a finite-sized lossy tissue region. Since standard FDTD equations pertinent to lossless and lossy dielectrics can be found elsewhere (see, for example, [25] and [26]) and a complete formulation of the method of analysis can be found in [27], only a brief summary of the major modeling considerations exercised is presented here.

The waveguide has a cross-sectional dimension of $a \times b$ centered around the origin in the $xy$-plane. The lossless dielectric filling the waveguide has a dielectric constant $\varepsilon_1$. A propagating $TE_{10}$ modal field, which varies sinusoidally in time at the frequency considered, is injected at the open-end of the waveguide at $z = 0$ (which is denoted as the "excitation plane" in Fig. 2). By placing the excitation plane at the aperture, only scattered fields are simulated in the waveguide region [25]. Furthermore, since reflected, evanescent, higher-order (including cross-polarized) modes are expected, the waveguide region is truncated sufficiently far away from the aperture to ensure that only the reflected $TE_{10}$ modal field reaches and penetrates across the truncation plane. Since this field propagates along $-z$-axis with a known phase velocity, an exact lattice truncation condition can be devised easily once the time step is specified [28]. Finally, by comparing the steady-state peak magnitude of the time-varying reflected field, and time instant of its occurence, with those of the excitation waveform, dominant-mode reflection coefficient ($\rho$) can be determined.

Except for the aperture opening, tissue region is bounded by a plane perfect electric conductor (pec) at $z = 0$ plane. Mur's second-order absorption boundary conditions [29] are employed to terminate FDTD computation domain at the truncation planes shown in Fig. 2. For lattice points located at the waveguide-skin and skin-fat interfaces, average permittivity bewteen the two dielectrics involved is used in the FDTD equations [30]. Diffractions from the edges of aperture opening are treated using edge conditions developed by Mur [31].

Program execution is terminated once the sinusoidal steady-state response is achieved everywhere in problem space. Outputs of the program include: 1) the dominant-mode reflection coefficient $\rho$, 2) the magnitude and phase of the aperture field (or, if desired, anywhere inside the tissue region), 3) the average dissipated power density (i.e., $\sigma|\mathbf{E}|^2/2$ in W/m$^3$ with $\sigma$ and $|\mathbf{E}|$ representing respectively the conductivity and peak electric field strength) for each and every cell in the tissue region, and 4) the total average power leaks out of the truncation boundary in the tissue region. Time-averaged Poynting vectors are first calculated using steady-state tangential electric and magnetic

field intensities found on the truncation planes. Summing them up and multiplying the sum by the common cell area results in an estimate of the amount of power leaking through these truncation planes.

In the case where the spherical tumor is centered along $z$-axis, problem geometry becomes symmetrical with respect to both the $xz$- and $yz$-plane. For incident $TE_{10}$ mode having a y-directed electric field, structural symmetry suggests that the reflected wave can only contain $TE_{mn}$ and $TM_{mn}$ (i.e., cross-polarized) modes with odd $m$ and even $n$. These modes are characterized by having zero tangential magnetic (electric) field in $yz$-($xz$-) plane. As is also shown in Fig. 2, these symmetry properties can be realized simply by placing a pmc over the $yz$-plane at $x = 0$ and a pec over the $xz$-plane at $y = 0$. With the original problem space divided into four equal parts and FDTD field simulation needs only to be performed over any one of them; a significant saving in computer resource required is achieved.

### *B. Computation of Radiometric Signal*

Noise power received by a radiometer antenna can be quantified by antenna temperature $T_A$. Radiometric detectability is determined by the difference in antenna temperatures measured with and without the presence of the subcutaneous hot source (which exhibits a physical temperature differential $\Delta T$ with the surrounding normal tissue). For a meaningful detection, this radiometric temperature differential ($\Delta T_m$) has to be greater than the sensitivity of the radiometer (which is governed by receiver bandwidth, system noise temperature, and integration time).

By dividing the hot source into $N$ cells, each with a subvolume $\Delta V_n (n = 1, 2, \ldots, N)$ and a physical temperature differential $\Delta T_n$, then from [5] and [6], $\Delta T_m$ can be written as

$$\Delta T_m = \sum_{n=1}^{N} C_n \Delta T_n \tag{1}$$

where $C_n$ denotes the radiometric weighting factor associated with the *nth* tumor cell. In view of antenna reciprocity, $C_n$ is found to be the same as the fraction of power carried by the incident $TE_{10}$ modal field (when the probe radiates) that is dissipated in the same tissue cell. Taking the finite radiometer bandwidth into consideration, $C_n$ can be found from

$$C_n = \frac{1}{B} \int_{f_o - B/2}^{f_o + B/2} \frac{P_{\text{abs}}(n; f)}{P_{\text{in}}(f)}\, df \tag{2}$$

where $f_o$ and $B$ represent the center frequency and bandwidth of the radiometer, and $P_{\text{in}}(f)$ and $P_{\text{abs}}(n, f)$ denote, respectively, the power carried by the incident $TE_{10}$ modal field and the power absorbed by the tissue constituting the $n$th cell at any frequency within the radiometer band. In this paper, the integrand shown in (2) is determined at 5 to 7 frequency points within the radiometer bandwidth and then integrate numerically. In these calculations, $P_{\text{in}}(f)$ is assigned a fixed value (typically, 0.1 mw) and, from which, the magnitude of the excitation waveform is then determined and used in the FDTD field calculations. The absorbed power is obtained simply by multiplying cell volume (which is constant throughout the entire FDTD lattice) by the corresponding dissipated power density derived from the FDTD field analysis program.

Use of (2) in (1) simulates the operation of a conventional radiometer for which the strength of radiometric signal is affected by the degree of signal reflection off the probe aperture. Consider for example the simpler case of a probe observing a semi-infinite lossy medium having a homogeneous temperature $T$. If the probe is matched perfectly with the medium, i.e., $|\rho| = 0$, then it will radiate/receive all energy into/from the lossy medium. Since the medium is isothermal, $T_A = T$ is expected. On the other extreme, probe will radiate/receive no energy into/from the medium if $|\rho| = 1$, which results in $T_A = 0$. In between the two extremes, as is usually the case found in practical situation, $T_A < T$ occurs.

It is obvious that physical temperature of a semi-infinite lossy and isothermal medium can be recovered from the measured $T_A$ if $|\rho|$ is known. Several techniques have been developed which enable the radiometer to determine the degree of reflection and compensate for it while performing radiometric measurement (see, for example, [23]). In this operation mode, $C_n$ becomes

$$C_n = \frac{1}{B} \int_{f_o - B/2}^{f_o + B/2} \frac{P_{\text{abs}}(n, f)}{P_{\text{trans}}(f)}\, df \tag{3}$$

where $P_{\text{trans}}(f) = (1 - |\rho(f)|^2) P_{\text{in}}(f)$ represents the actual power transmitted across the radiating probe aperture into the tissue medium. It is obvious that the two $C_n$'s defined in (2) and (3) represent, respectively, the position-dependent (and frequency-averaged) near-field power gain and directivity of the waveguide probe considered here.

While this latter approach works fine for problems involving an isothermal lossy half space (as evidenced by the experimental results shown in [23]), there simply exists no simple way to assign "fractional" reflection coefficients to individual layers in a near-field environment. Therefore, results to be presented in the followings are all computed from (1) and (2).

## III. Numerical Results

Results obtained from the present method of analysis for a 3-GHz band radiometer observing a distilled-water tank that contains a spherically shaped hot source are found to be in good agreement with data reported in [5] and [6]. Since structural parameters and frequency range considered are different from the problem of interest here, results of that verification experiment and additional 3-GHz radiometry data are reported in a separate paper [32].

For the 10-GHz radiometry data presented in this section, the following common parameters are used: 1) uniform FDTD cell of cubic shape having a sidelength $\Delta = 5/90$ cm $\approx$ 0.556 mm and a common cell volume $\Delta V_n$ of $1.7147 \times 10^{-10}$ m$^3$ is used throughout the entire FDTD lattice, 2) waveguide is filled with alumina ($\varepsilon_{r1} = 9.72 - j0$) and has a cross section ($a \times b$) measuring $16\Delta \times 8\Delta (\approx 8.89 \text{ m/m} \times 4.45 \text{ m/m}$, which results in a $TE_{10}$ mode cut off frequency of 5.413 GHz), 3) skin has a complex dielectric constant of $\varepsilon_{r2} = 40.0 - j12.3$ and a thickness of $3\ \Delta (\approx 1.67$ mm),

TABLE I
POWER TRANSIMITTED ACROSS THE APERTURE VERSUS POWER ABSORBED BY THE TISSUE AND POWER FLOWS OUT OF THE TRUNCATED PLANES IN THE TISSUE REGION. NORMALIZATION IS MADE AGAINST THE POWER CARRIED BY THE INCIDENNT $TE_{10}$ MODAL FIELD

| Tissue Type | Frequency (GHz) | Normalized Transmitted Power | Normalized Absorbed Power | Normalized Power Flows Out of the Truncation Planes |
|---|---|---|---|---|
| Fat Only | 9.5 | 0.857 | 0.860 | 0.02 |
| | 10.0 | 0.869 | 0.871 | 0.0175 |
| | 10.5 | 0.878 | 0.877 | 0.015 |
| Skin Plus Fat | 9.5 | 0.706 | 0.695 | 0.0019 |
| | 10.0 | 0.737 | 0.725 | 0.0018 |
| | 10.5 | 0.773 | 0.764 | 0.0017 |

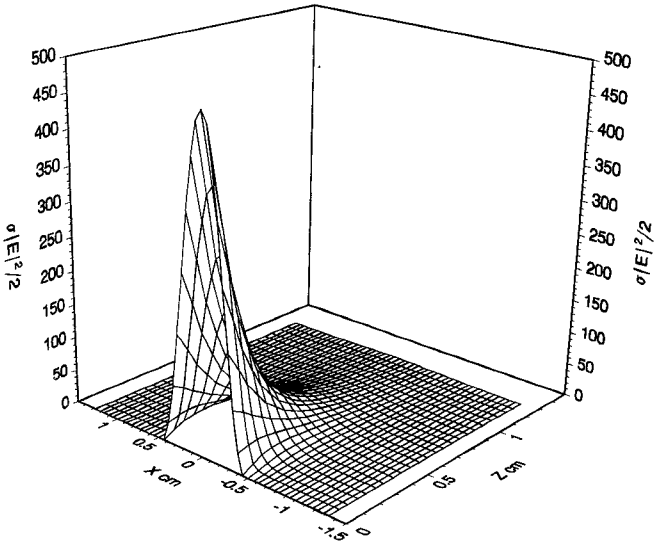


(a)

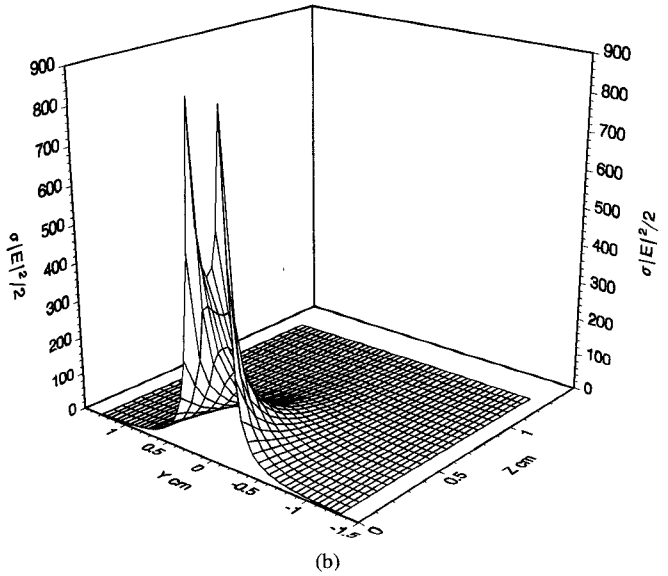


(b)

Fig. 3. 3-D absorbed power density patterns in: (a) $xz$-plane ($y = 0$) and (b) $yz$-plane ($x = 0$); fat only.

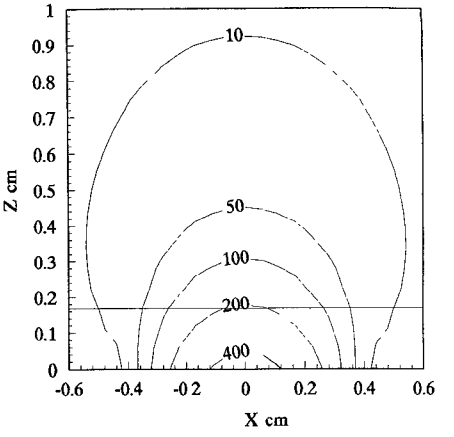


(a)

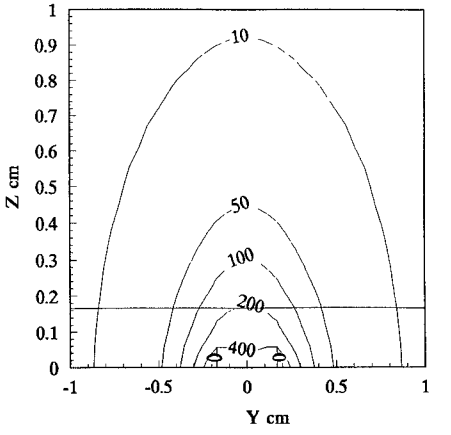


(b)

Fig. 4. Contour plots of the absorbed power density patterns in: (a) $xz$-plane ($y = 0$), and (b) $yz$-plane ($x = 0$); fat only. Locations of maximum absorbed power density of 892.743 W/m$^3$ are denoted by rotated "0" symbol in (b).

and 4) fat has a complex dielectric constant of $\varepsilon_{r3} = 4.5 - j0.79$. Dielectric data for skin and fat are estimated from data tabulated at [33]. Effects of skin layer are demonstrated using data obtained for the case of fat-only tissue model as references. To ease the computational efforts, only symmetrical cases of spherical tumors of various size and depth centered along the $z$-axis are considered; this symmetry also suggests that $TE_{30}$ mode that cutoffs at 16.239 GHz is the first reflecting high-order waveguide mode. Due to small cell size and time step used, a CPU time of about 3 hrs. is needed to obtain the 3-D radiometric weighting function at each frequency point when running on a HP 9000/755 workstation.

As a first example, power transmitted out of the waveguide opening evaluated from the dominant-mode reflectivity $|\rho|^2$, total power absorbed by tissues contained in the finite FDTD lattice, and power flows out of the truncation planes in tissue region are tabulated in Table I. These data are normalized with respect to the power carried by the incident $TE_{10}$ modal field. Results shown are obtained at 9.5, 10.0, and 10.5-GHz, which represent the center frequencies of three radiometers each having a 500-MHz bandwidth. As can be seen that, in all cases, the majority of the transmitted power are absorbed in the finite tissue region simulated and only a very small percentage of power flows out of the exterior truncation planes (especially when the highly-lossy skin is present). Table I further reveals that the presence of the skin layer produces approximately a

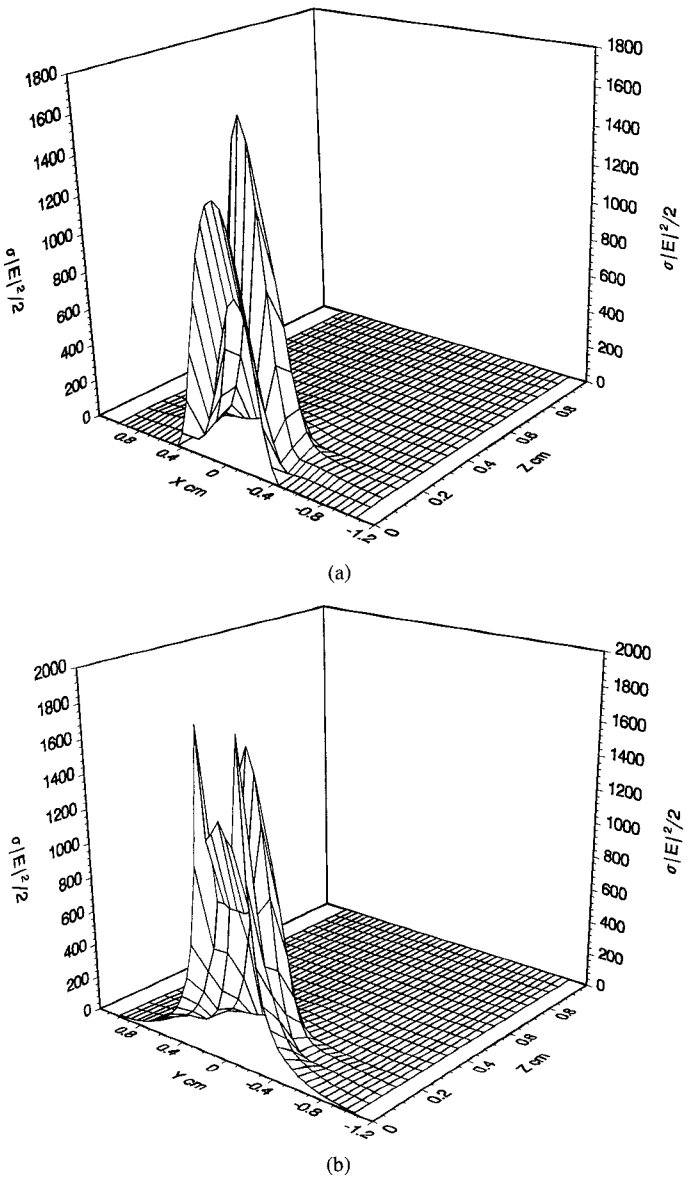


Fig. 5. 3-D absorbed power density patterns in: (a) $xz$-plane ($y = 0$), and (b) $yz$-plane ($x = 0$); skin plus fat.

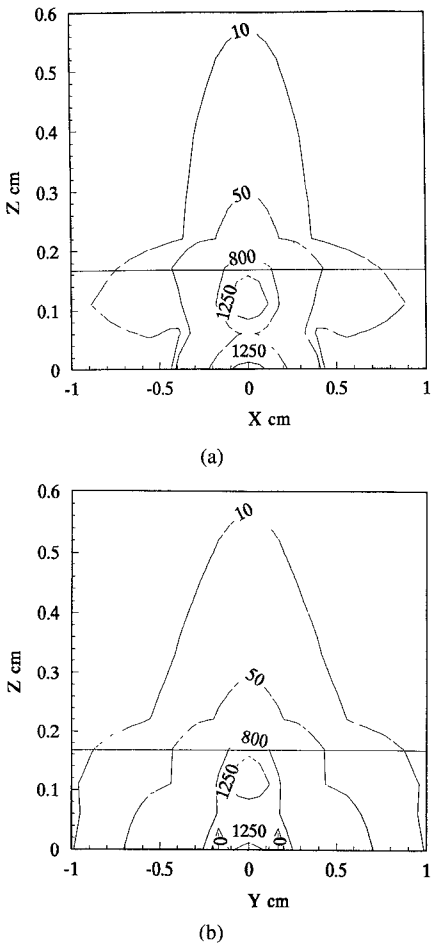


Fig. 6. Contour plots of the absorbed power density patterns in: (a) $xz$-plane ($y = 0$), and (b) $yz$-plane ($x = 0$); skin plus fat. Locations of maximum absorbed power density of 1835.338 W/m$^3$ aredenoted by rotated "0" symbol in (b). Horizontal line appearing at $z = 0.167$ cm in both (a) and (b) denotes skin-fat interface.

15% reduction in the power transmitted across the aperture; same percentage reduction in $T_A$ also exists in radiometer measurement. Excellent power balance between the waveguide and tissue regions and rather small amount of power leaking through the exterior truncation boundary also attest to the quality of the FDTD-derived active probe characteristics.

Next we consider the homogeneous fat tissue case. Three-dimensional plots of the absolute absorbed power density (in W/m$^3$) data obtained over the two symmetry planes at $x = 0$ and $y = 0$ are shown in Fig. 3 and the corresponding contour plots are shown in Fig. 4. As expected, strong edge diffractions occur near the central portion of the upper and lower edges of the aperture in $yz$-plane. Two mirror-imaged locations where the maximum power density of 892.743 W/m$^3$ occurred are marked by the rotated "0" symbol in Fig. 4(b). Furthermore, rapidly decreasing power patterns found in the two transverse directions should also justify our use of plane layers tissue model.

Corresponding 3-D and 2-D contour plots of the absorbed power density patterns calculated after the addition of a 1.67-mm-thick skin layer are shown in Figs. 5 and 6, respectively. Apparently due to skin's much higher complex permittivity and its immediate proximity to the aperture, much higher (than the fat-only case) absorbed power densities occurred in the skin layer. Moreover, rapid spatial power variations, especially in the region between the aperture and skin-fat interface, found in these plots clearly demonstrate the highly complicated nature of near-field interactions between the probe and the bilayered media.

Effects of skin layer on the magnitude and phase distributions of the $y$-component of the aperture field along $y$-axis and $x$-axis are illustrated in Figs. 7 and 8, respectively. These data are obtained at 10.0 GHz and normalizations are made with respect to the magnitude and phase values of the $E_y$ found at the center of the aperture. Changes in both the magnitude and phase distributions are clearly observed which can be attributed to the generations of higher-order waveguide modes. Focal shift will occur if these effects are not taken into account when designing an aperture phase-correction lens for use with focused hyperthermia.

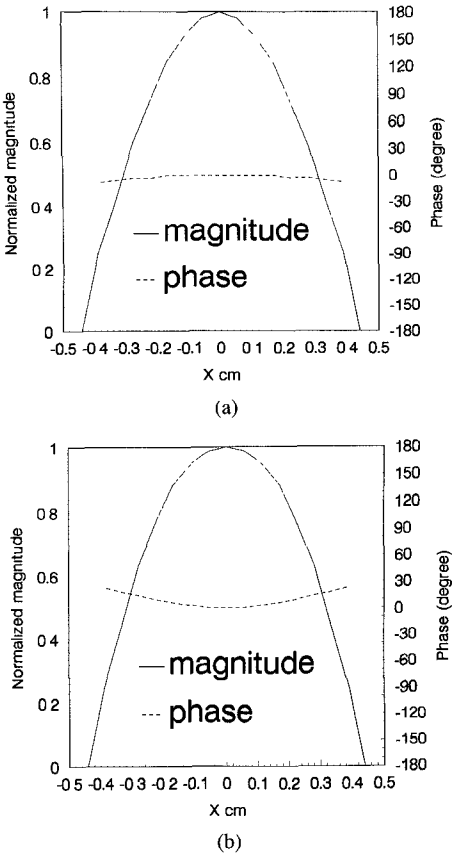


Fig. 7. Normalized magnitude and phase distributions of $E_y$ along the $y$-axis across the aperture ($z = 0$ cm) for: (a) fat only, and (b) skin plus fat.

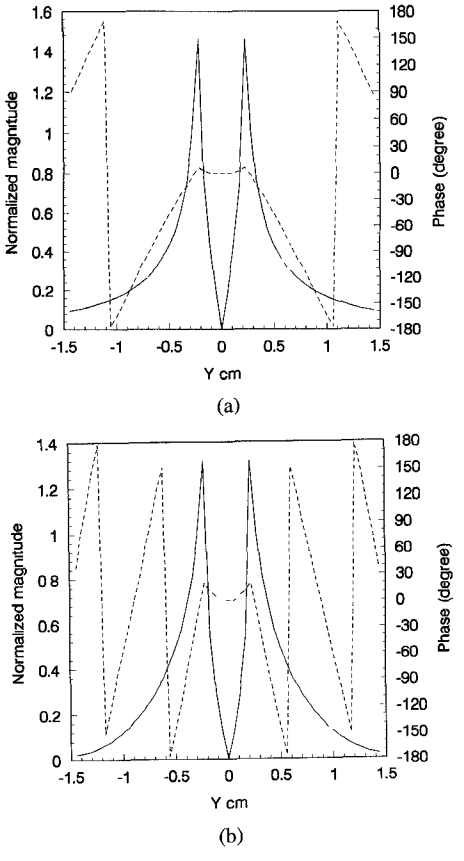


Fig. 9. Normalized magnitude and phasedistributions of $E_z$ along the $y$-axis with $x = 0$ and $z = 0.28$ mm for: (a) fat only, and (b) skin plus fat.

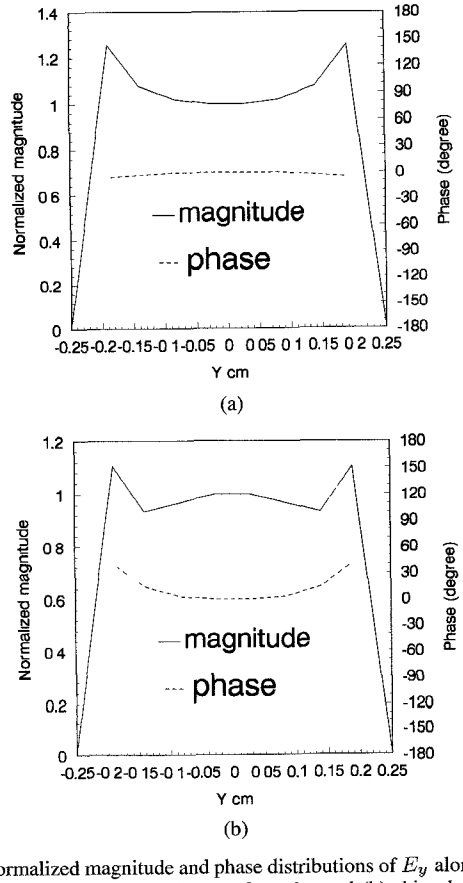


Fig. 8. Normalized magnitude and phase distributions of $E_y$ along the $x$-axis acrossthe aperture ($z = 0$ cm) for: (a) fat only, and (b) skin plus fat.

While $E_y$ (and $E_x$) assumes zero value over the entire pec plane where the aperture is mounted, behavior of the non-zero normal field component (i.e., $E_z$) over this plane is also of interest. $E_z$'s computed at half-cell deep into the skin layer (i.e., $z \approx 0.28$ mm) and along the $y$-axis where $x = 0$ are plotted in Fig. 9. Whether skin is present or not, $|E_z|$ increases rapidly from zero value at the center of the aperture ($y = 0$) to the maximum at the edge of the aperture ($y = \pm 0.45$ cm). As $y$ increases further, especially when the highly-lossy skin layer is present, $|E_z|$ decreases very rapidly. Skin's much higher dielectric constant also causes the phase of $E_z$ to vary much more rapidly. The rapidly peaking phenomena found for both $|E_y|$ and $|E_z|$ nearing the two edges of the aperture along $\pm y$-axis fade away rapidly as $z$ increases [27], which echos the highly localized nature of edge diffraction.

Finally, effects of skin on radiometric signal are demonstrated in Figs. 10 and 11 for a radiometer with a 500-MHz bandwidth centered around 10 GHz. For isothermal tumor assumed here, calculated radiometric temperature differential $\Delta T_m$ is normalized to the tumor's physical temperature differential $\Delta T$. Tumor diameters of 0.56- , 1.00- , 1.56- , and 2.00-cm are considered. Results are obtained for tumor depth below the center of the waveguide opening (i.e., $z = t + d$ for the geometry shown in Fig. 1) ranges from just below the skin layer (i.e., $z = 0.16875$ cm) and up to 2.2 cm. Since tumor permittivity is assumed to be the same as that of the normal fat tissue, radiometric signals are found to increase with tumor size and decreases with tumor depth in both cases. However,

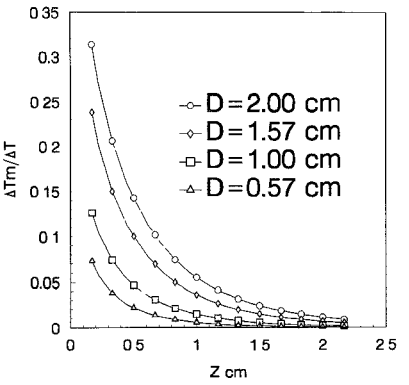


Fig. 10. Normalized radiometric signal versus tumor depth and diameter; fat only.

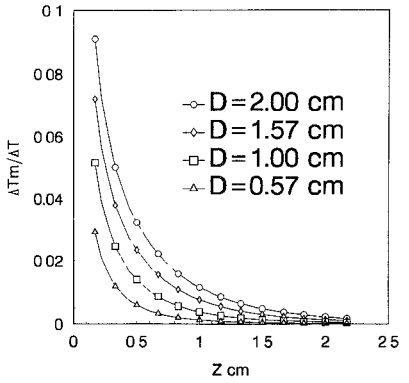


Fig. 11. Normalized radiometric signal versus tumor depth and diameter; skin plus fat.

presence of skin layer is found to produce an almost 3-fold decrease in radiometric signal for all tumor sizes considered; similar observations are also found at 9.5- and 10.5-GHz bands [27]. Obviously, reduced power transmission coefficent and much lower power absorbed by fat tissue found in Table I and Fig. 6 can also explain the much lower radiometric signals observed here when skin is present.

## IV. Conclusion

Total power radiometer observation of spherical hot source representation of a tumor in a bilayered biological tissue media is analyzed using the FDTD method in this paper. Absorbed power patterns suggest that the use of planar two-layer structure is judicious for the $X$-band dielectric-filled waveguide probe considered.

Significant changes in both the aperture field distributions and absorbed power patterns (and radiometric weighting functions) inside the tissue region are observed when considering the presence of a thin, highly lossy, skin layer. Therefore, effects of skin should be taken into account when designing probes for use in subcutaneous microwave hyperthermia and radiometry. Perhaps the most devastating effect observed when the skin is present is the almost 3-fold reduction in radiometric signals found for all tumor parameters examined. It means low radiometric signal strength and poor detectability when the tumor is small in size and/or having small $\Delta T$.

To increase the strength of radiometric signal, probes with better impedance matching performance and signal penetration depth than the one employed here are highly desired. These may be found in larger-sized waveguide probes filled with material having a higher dielectric constant (than that of the alumina considered here) and operating at lower frEquencies. In doing so, however, factors such as conformity between the finite-sized ground plane and curved body surface and presence of deeper non-fatty breast tissues (see, for example, [34]) should be considered. Extension of the present FDTD method to accomodate these operational considerations is currently underway. Results of which will be reported in the future.

## References

[1] A. H. Barret, P. C. Myers, and N. L. Sadowski, "Detection of breast cancer by microwave radiometry," *Radio Sci.*, vol. 12, pp. 167–171, 1977.

[2] K. L. Carr, "Microwave radiometry: Its importance to the detection of cancer," *IEEE Trans. Microwave Theory Tech.*, vol. 37, pp. 1862–1869, Dec. 1989.

[3] B. Bocquet, A. Mamouni, M. Hochedez, J. C. van de Velde, and Y. Leroy, "Visibility of local thermal structures and temperature retrieval by microwave radiometry," *Electron. Lett.*, vol. 22, no. 3, pp. 120–122, Jan. 1986.

[4] B. Bocquet, J. C. van de Velde, A. Mamouni, Y. Leroy, G. Giaux, J. Delannoy, and D. Delvalee, "Microwave radiometric imaging at 3 GHz for the exploration of breast tumors," *IEEE Trans. Microwave Theory Tech.*, vol. 38, pp. 791–793, June 1990.

[5] A. Mamouni, Ph. Gelin, and Y. Leroy, "Modeling of radiometric signals for medical applications," in *Proc. 18th Euro. Microwave Conf.*, Stockholm, 1988, pp. 632–637.

[6] A. Mamouni, Y. Leroy, B. Bocquet, J. C. van de Velde, and Ph. Gelin, "Computation of near-field microwave radiometric signals: Definition and experimental verification," *IEEE Trans. Microwave Theory Tech.*, vol. 39, pp. 124–132, Jan. 1991.

[7] B. Bocquet, P. DeHour, A. Mamouni, J. C. van de Velde, and Y. Leroy, "Near field microwave radiometric weighting functions for multilayered materials," *J. Electromagn. Waves Appl.*, vol. 7, no. 11, pp. 1497–1514, 1993.

[8] D. V. Land, "Radiometer receivers for microwave thermography," *Microwave J.*, vol. 26, no. 5, pp. 196–201, May 1983.

[9] J. C. Hill and R. B. Goldner, "The thermal and spatial resolution of a broad-band correlation radiometer with application to medical microwave thermography," *IEEE Trans. Microwave Theory Tech.*, vol. 33, pp. 718–722, Aug. 1985.

[10] N. C. Haslam, A. R. Gillespie, and C. G. T. Haslam, "Aperture synthesis thermography—A new approach to passive microwave temperature measurements in the body," *IEEE Trans. Microwave Theory Tech.*, vol. 32, pp. 829–835, Aug. 1984.

[11] F. Bardati, M. Mongiardo, and D. Solimini, "Synthetic array for radiometric retrieval of thermal fields in tissues," *IEEE Trans. Microwave Theory Tech.*, vol. 34, pp. 579–583, May 1986.

[12] F. Bardati, V. J. Brown, and P. Tognolatti, "Temperature reconstructions in a dielectric cylinder by multi-frequency microwave radiometry," *J. Electromagn. Waves Appl.*, vol. 7, no. 11, pp. 1549–1571, 1993.

[13] G. Schaller, "On the imaging of hot spots using correlation radiometers and a circular aperture," *IEEE Trans. Microwave Theory Tech.*, vol. 37, pp. 1210–1216, Aug. 1989.

[14] R. U. K. Noell, K. Woodward, B. Worde, R. Fishburn, and L. Miller, "Microwave-induced local hyperthermia in combination with radiotherapy of human malignant tumors," *Cancer*, vol. 45, pp. 638–646, 1980.

[15] K. L. Carr, A. M. El-Mahdi, and J. Shaeffer, "Dual-mode microwave system to enhance early detection of cancer," *IEEE Trans. Microwave Theory Tech.*, vol. 29, pp. 256–260, Mar. 1981.

[16] C. H. Durney and M. F. Iskander, "Antennas for medical applications," in *Antenna Handbook: Theory, Applications and Design*, Y. T. Lo and S. W. Lee, Eds. New York: Van Norstrand Reinhold, 1988, ch. 24.

[17] C. H. Durney, "Antennas and other electromagnetic applicators in biology and medicine," *Proc. IEEE*, vol. 80, pp. 194–199, Jan. 1992.

[18] J. Montreuil and M. Nachman, "Multiangle method for temperature measurement of biological tissues by microwave radiometry," *IEEE Trans. Microwave Theory Tech.*, vol. 39, pp. 1235–1239, July 1991.

[19] A. W. Guy, "Electromagnetic fields and relative heating patterns due to a rectangular aperture source in direct contact with bilayered tissue," *IEEE Trans. Microwave Theory Tech.*, vol. 19, pp. 214–223, Feb. 1971.
[20] E. Alanen and I. V. Lindell, "Effects of skin in microwave detection of breast cancer," *IEEE Trans. Microwave Theory Tech.*, vol. 34, pp. 584–588, May 1986.
[21] V. Teodoridis, T. Sphicopoulos and F. E. Gardiol, "The reflection from an open-ended rectangular waveguide terminated by a layered dielectric medium," *IEEE Trans. Microwave Theory Tech.*, vol. 33, pp. 359–366, May 1985.
[22] K. S. Yee, "Numerical solution of initial boundary value problems involving Maxwell's equations in isotropic media," *IEEE Trans. Antennas Propagat.*, vol. 14, pp. 302–307, May 1966.
[23] A. Mamouni, F. Bilot, Y. Leroy, and Y. Moschetto, "A modified radiometer for temperature and microwave properties measurements of biological substances," in *Proc. 7th Euro. Microwave Conf.*, Copenhagen, 1977, pp. 703–707.
[24] A. Mamouni, Y. Leroy, J. C. van de Velde, and L. Bellarbi, "Introduction to correlation microwave thermography," *J. Microwave Power*, vol. 18, no. 3, pp. 285–293, 1983.
[25] A. Taflove and K. R. Umashankar, "Review of FDTD numerical modeling of electromagnetic wave scattering and radar cross section," *Proc. IEEE*, vol. 77, pp. 682–699, May 1989.
[26] P. C. Cherry and M. F. Iskander, "FDTD analysis of power deposition patterns of an array of interstitial antennas for use in microwave hyperthermia," *IEEE Trans. Microwave Theory Tech.*, vol. 40, pp. 1692–1699, Aug. 1992.
[27] W. K. Nieh, "FDTD analysis of radiation into lossy multi-layered halfspace from an open-ended rectangular waveguide with grounded side wall and its application on microwave radiometry," M.S. thesis, Institute of Communication Engineering, National Chiao Tung University, Hsinchu, Taiwan, June 1994.
[28] L. K. Wu and F. R. Wang, "Analysis of inductive dielectric posts in rectangular waveguide using finite-difference time-domain method," in *Proc. 1991 PIERS*, Cambridge, MA, p. 563.
[29] G. Mur, "Absorbing boundary conditions for the finite-difference approximation of the time-domain electromagnetic-field equations," *IEEE Trans. Electromagn. Compat.*, vol. 23, pp. 377–382, Nov. 1981.
[30] X. Zhang and K. K. Mei, "Time-domain finite difference approach to the calculation of the frequency-dependent characteristics of microstrip discontinuities," *IEEE Trans. Microwave Theory Tech.*, vol. 36, pp. 1775–1787, Dec. 1988.
[31] G. Mur, "The modeling of singularities in the finite-difference approximation of the time-domain electromagnetic-field equations," *IEEE Trans. Microwave Theory Tech.*, vol. 29, pp. 1073–1077, Oct. 1981.
[32] L. K. Wu and W. K. Nieh, "Potential effects of glass container on radiometric measurements of liquid tissue phantom," in preparation.
[33] M. A. Stuchly and S. S. Stuchly, "Dielectric properties of biological substances—Tabulated," *J. Microwave Power*, vol. 15, pp. 19–26, 1980.
[34] A. M. Campbell and D. V. Land, "Dielectric properties of female human breast tissue measured in vitro at 3.2 GHz," *Phys. Med. Bio.*, vol. 37, no. 1, pp. 193–210, 1992.

**Lin-Kun Wu** (S'81-M'81–S'81–M–'85) received the Ph.D. degree in electrical engineering from the University of Kansas in 1985.

From November 1985 to December 1987, he was a Postdoctoral Research Associate at the Center for Research, Inc. of the University of Kansas working on microwave remote sensing and computational electromagnetics. In 1988, he joined the Department of Communication Engineering, National Chiao Tung University, where he's currently a Professor. His current research interests include computational electromagnetics and biological effects and medical applications of electromagnetic energy.

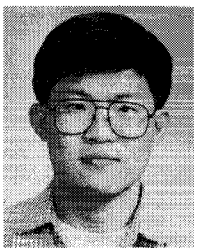

**William K. Nieh** (S'92-M'94) received the B.S. and M.S. degrees from the Department of Communication Engineering, National Chiao Tung University, in 1989 and 1994, respectively.

From 1991 to 1992, he was a Teaching Assistant at the Department of Electronics Engineering, National Chiao Tung University. Since July 1994, he has been an Electronic Engineer at the Microelectronic Technology Inc., Hsinchu, Taiwan. His current interests are microelectronic circuits, electromagnetics and communication system technologies.